JOURNAL OF CATALYSIS 136, 493–503 (1992)

Regulation of Reaction Intermediate by Reactant in the Water–Gas Shift Reaction on CeO_2, in Relation to Reactant-Promoted Mechanism

TAKAFUMI SHIDO[1] AND YASUHIRO IWASAWA[2]

Department of Chemistry, Faculty of Science, the University of Tokyo, Hongo, Bunkyo-ku, Tokyo 113, Japan

Received November 25, 1991; revised March 12, 1992

Reaction regulation by intermediate-reactant interaction in the water–gas shift reaction (H_2O + CO → H_2 + CO_2; WGSR) on CeO_2 was investigated in relation to the reactant-promoted mechanism on MgO and ZnO by FT-IR. Terminal OH groups on partially reduced CeO_2 reacted with CO to produce bridge formates. Bridge formates were converted to bidentate formates above 443 K, and this transformation occurred at room temperature when water coexisted. The decomposition of the surface formates was affected by the water molecule; 70% of the bidentate formates decomposed to OH + CO (backward decomposition) and 30% of them decomposed to H_2 + CO_2 (forward decompose to H_2 and unidentate carbonates. The decomposition of the unidentate carbonates to CO_2 was promoted by coadsorbed water. The results are also discussed in comparison with the formates increased from 94 kJ mol^{-1} without water to 193 kJ mol^{-1} with water. Isotope effects were observed on the hydrogen atoms of both formate and hydroxyl, giving a proposed transition state in the reaction mechanism. The bidentate formates reacted with the adjacent hollow-site OH to decompose to H_2 and unidentate carbonates. The decomposition of the unidentate carbonates to CO_2 was promoted by coadsorbed water. The results are also discussed in comparison with the results for WGSR on MgO and ZnO.

INTRODUCTION

Promoting effects of CeO_2 in many catalytic reactions have been investigated (*1–8*). CeO_2 has also been demonstrated to be a reservoir of oxygen in catalytic reactions (*9–11*). CeO_2-supported metal catalysts, on the other hand, catalyze the water–gas shift reaction (WGSR: CO + H_2O → CO_2 + H_2) (*2, 4, 5, 12*). WGSR itself is not only an important chemical process, but also one of the key steps involved in automobile exhaust processes.

In the previous papers, we reported the reactant-promoted reaction mechanism for WGSR on MgO and ZnO, where the activation of surface formates by coadsorbed water is necessary to catalytically proceed WGSR (*13, 14*). Surface formates have been demonstrated to be the intermediates of WGSR (*15, 16*), methanol decomposition (*17*), and formic acid decomposition (*18*). Thus, it may be of great interest to clarify the behavior of surface formate intermediates activated by reactants in order to understand essential factors for the genesis of solid catalysis.

The surface formates produced from OH groups and CO can be characterized by means of IR: The adsorption sites of the formates are estimated by ν(OH) of hydroxyls that react with CO to produce the formates (*19–21*) and the structures of the formates are determined by the difference of ν_{as}(OCO) and ν_s(OCO) (*13, 14, 22*).

On MgO, terminal hydroxyls react with CO to form unidentate, bidentate (few), and bridge formates. All of the surface formates

[1] Present address: Catalysis Research Center, Hokkaido University, Sapporo 060, Japan.

[2] To whom correspondence should be addressed.

0021-9517/92 $5.00

decomposed to CO and hydroxyls (backward reaction) in vacuum. When water coexists, unidentate formate changed to bridge formate, and the bridge formate (100%) was converted to CO_2 + H_2 (forward reaction) (*13*). On the contrary, surface formates on ZnO were of bidentate type; 70% of them decomposed to OH + CO and 30% of them decomposed to H_2 + CO_2 in vacuum. When water coexisted, 100% of the formates were converted to WGSR product CO_2 + H_2 (*14*).

Surface formates have been reported to be produced by the reaction of CO and surface hydroxyl groups on partially reduced CeO_2 (*23*). In the present paper we investigated the properties of surface formates and the interaction between the formates and coadsorbed water on CeO_2, in relation to the reactant-promoted reaction mechanism.

EXPERIMENTAL

CeO_2 was obtained by calcination of $Ce(OH)_4$ at 773 K for 4 h. $Ce(OH)_4$ was obtained by the precipitation from aqueous solution of $Ce(NO)_3$ (99%) with NH_{3aq}. Surface area of the obtained CeO_2 was 111 m^2 g^{-1} by BET measurement with N_2 adsorption. CeO_2 was oxidized at 773 K for 1 h followed by evacuation at 773 K for 1 h. CeO_2 was further reduced by hydrogen at 623 K or given temperatures to obtain partially reduced CeO_2. Finally, the sample was exposed to water vapor at 473 K, followed by evacuation at 623 K, to introduce hydroxyl groups on the surface. To achieve the introduction of OD groups on the CeO_2 surface, the sample was reduced with D_2 and exposed to D_2O. Table 1 shows the notation for the samples treated in different ways. For example, CeO_2 (R, OD) represents the CeO_2 reduced at 623 K and exposed to D_2O vapor.

IR, TPD, and kinetic studies were performed in a similar way to that described in the previous papers (*13, 14, 21*). Ca. 40 mg of CeO_2 was pressed into a self-support disk in 20 mm diameter. The disc was mounted in an IR cell which was combined in a closed circulating system. IR spectra were measured at given temperatures with resolution of 2 or 4 cm^{-1}.

TABLE 1

Pretreatment Processes of CeO_2

Notation	Pretreatment
CeO_2 (O, OH)	Oxidized at 773 K, exposed to H_2O, followed by evacuation at 623 K.
CeO_2 (O, OD)	Oxidized at 773 K, exposed to D_2O, followed by evacuation at 623 K.
CeO_2 (R, OH)	Reduced at 623 K, exposed to H_2O, followed by evacuation at 623 K.
CeO_2 (R, OD)	Reduced at 623 K, exposed to D_2O, followed by evacuation at 623 K.
CeO_2 (RR, OH)	Reduced at 723 K, exposed to H_2O, followed by evacuation at 623 K.
CeO_2 (RR, OD)	Reduced at 723 K, exposed to D_2O, followed by evacuation at 623 K.

RESULTS

1. IR Spectra

Figure 1a shows IR spectra of adsorbed CO species on CeO_2 (O, OD). When the CeO_2 was exposed to CO at 303 K, bands at 1560, 1505, 1280, and 1050 cm^{-1} appeared. When the sample was exposed to CO at 373 K, other bands at 1394 and 1344 cm^{-1} appeared. At 513 K the bands at 2156, 1540, 1500, 1394, and 1344 cm^{-1} were observed. Figure 1b shows IR spectra of adsorbed CO species on CeO_2 (R, OD). When the CeO_2 was exposed to CO at 303 K, the bands at 2156 and 2140 cm^{-1} in the ν(CD) region, 1560, 1540, and 1510 cm^{-1} in the ν_{as} (OCO) region, and 1332 cm^{-1} in the ν_s(OCO) region were observed. Above 373 K, the intensity of these bands increased and new bands appeared at 1466 and 1384 cm^{-1}. The assignments of IR bands are listed in Table 2. The assignments are described hereinafter.

Figure 2 shows the IR spectra of surface formates on CeO_2 (R, OD). When the evacu-

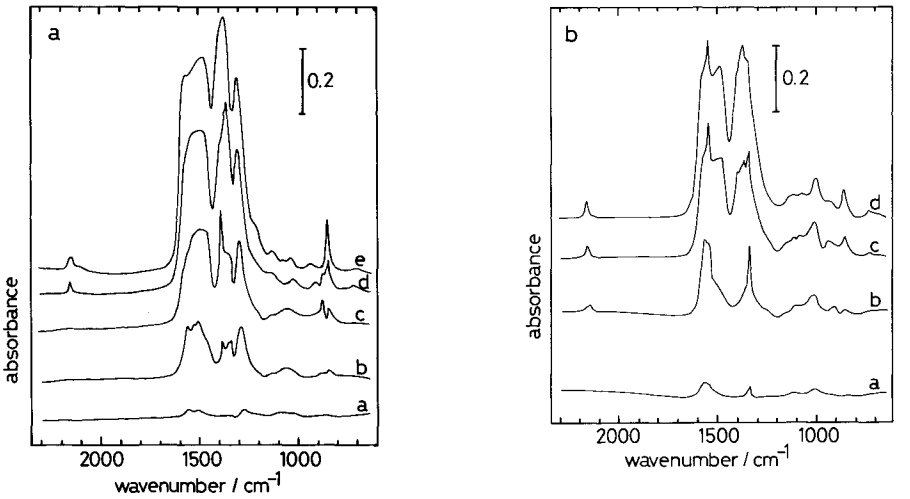

FIG. 1. [a] IR spectra of adsorbed species on CeO_2 (O, OD); the sample was exposed to 4.0 kPa of CO at (a) 303 K, (b) 373 K, (c) 443 K, (d) 513 K, and (e) 583 K. [b] IR spectra of adsorbed species on CeO_2 (R, OD); the sample was exposed to 4.0 kPa of CO at (a) 303 K, (b) 373 K, (c) 443 K, and (d) 513 K.

ation temperature increased from 373 to 543 K, the peaks at 2140, 1560, and 1332 cm^{-1} which are attributed to bridge formate shifted to 2156, 1540, and 1338 cm^{-1}, which are assigned to bidentate formate. When the sample was evacuated at 613 K, the bands of 2156, 1540, and 1338 cm^{-1} vanished. The intensity of bands at 1466 and 1384 cm^{-1} increased as the evacuation temperature increased up to 613 K.

TABLE 2

IR Absorption Bands of Adsorbed Species on CeO_2

Species	IR bands (cm^{-1})
Bidentete formate[a]	ν(CH), 2845(2156); ν_{as}(OCO), 1547(1540); ν_s(OCO), 1358(1338)
Bridge formate[a]	ν(CH), 2933 (2140); ν_{as}(OCO), 1569(1560); ν_s(OCO), 1358 (1332)
Unidentate carbonate	ν_{as}(OCO), 1460; ν_s(OCO), 1370; ν(CO), 1044
Bidentate carbonate	ν(C=O), 1570; ν_{as}(OCO), 1286[b]; ν_s(OCO), 1028[b]
Carboxylate	ν_{as}(OCO), 1510; ν_s(OCO), 1310[b]

[a] The values in parentheses are those for DCOO.
[b] Tentatively assigned, due to the overlapping with other bands.

Figure 3 shows the change of IR spectra of surface formates on CeO_2 (R, OD) by exposing the sample to D_2O vapor. The conversion of bridge formate to bidentate formate was observed at 403–473 K. The temperature for the transformation of bridge formate to bidentate formate reduced by ca.

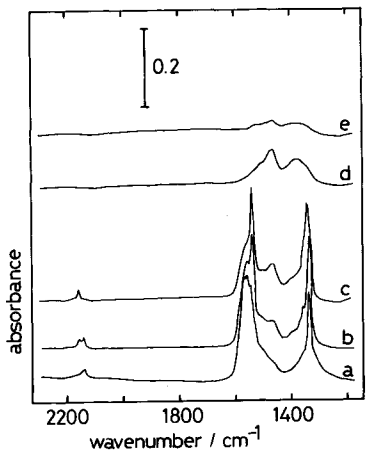

FIG. 2. IR spectra of surface formates (DCOO) on CeO_2 (R, OD); the sample was exposed to 4.0 kPa of CO at 373 K followed by evacuation at 373 K (a), 473 K (b), 543 K (c), 613 K (d), and 683 K (e).

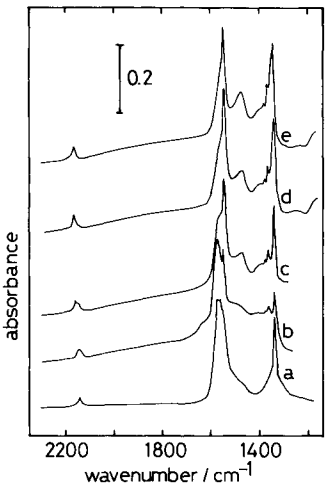

FIG. 3. IR spectra of surface formates (DCOO) on CeO_2 (R, OD); (a) the sample was exposed to 4.0 kPa of CO at 373 K followed by evacuation at 373 K. After (a), the sample was exposed to 0.66 kPa of D_2O at 303 K, followed by evacuation at (b) 303 K, (c) 403 K, (d) 473 K, and (e) 543 K.

100 K in the water coadsorption as compared to that without coadsorbed water.

Surface OD groups on CeO_2 (R, OD) exhibited the peaks at 2707, 2681, 2590 and 2540 cm^{-1} as shown in Fig. 4. When CO was admitted to the surface at 373 K, the intensities of the 2707- and 2540-cm^{-1} peaks decreased and the intensity at 2590 cm^{-1}

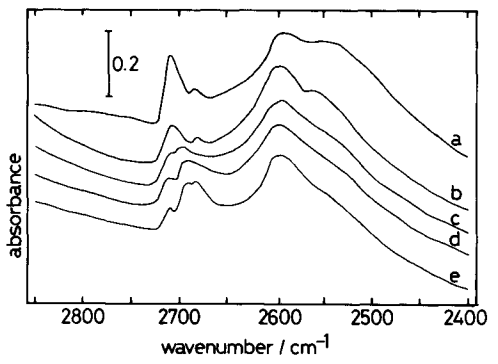

FIG. 4. IR spectra of surface OD groups on CeO_2 (R,OD): (a) after pretreatment; after (a) the sample was exposed to 4.0 kPa of CO at 373 K, followed by evacuation at 373 K (b), 503 K (c), 573 K (d) and 623 K (e).

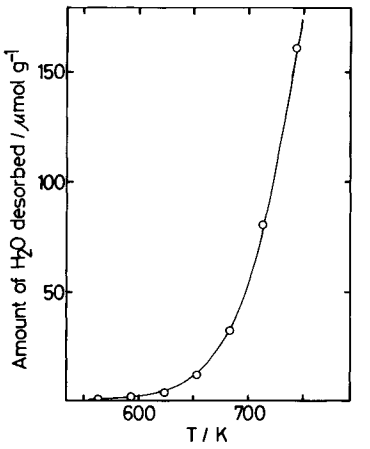

FIG. 5. Amount of produced water as a function of reduction temperature. CeO_2 was exposed to 4.0 kPa of hydrogen for 20 min at given temperatures.

increased. With an increase of evacuation temperature, the intensity of the 2707-cm^{-1} peak markedly decreased and that of the 2690-cm^{-1} peak newly developed.

2. *Temperature Programmed Desorption Experiments*

CeO_2 was reduced with H_2 to form H_2O. The amount of desorbed water was plotted as a function of reduction temperature in Fig. 5, where the sample was exposed to 4.0 kPa of H_2 at given temperatures for 20 min. The reduction of CeO_2 began at 573 K. When the sample was reduced at 623 K, 4 μmol of oxygen per gram of CeO_2 was removed. The amount corresponding to about one twentieth of surface oxygen atoms. At 743 K, H_2O equivalent to the surface monolayer oxygen of CeO_2 (160 μmol g^{-1}) was produced.

Figure 6 shows TPD spectra of surface formates on CeO_2 (R, OH). The sample was exposed to CO at 373 K then heated from room temperature to 773 K at a heating rate of 3 K min^{-1}. Desorption peaks of CO and H_2 appeared at 518 and 535 K, respectively. CO_2 desorbed above 710 K and had no peak below 773 K. The desorbed amounts of CO and H_2 were 28.4 and 11.6 μmol g^{-1}, respectively. Figure 7 shows TPD spectra of sur-

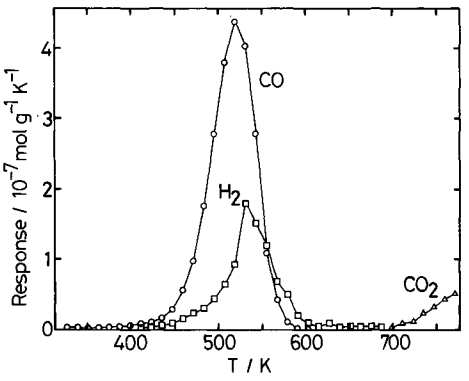

FIG. 6. TPD spectra of surface formates on CeO_2 (R, OH) in vacuum, (○) CO, (□) H_2, and (△) CO_2.

face formates on CeO_2 (R, OH) under 0.67 kPa of H_2O. The pretreatment and heating rate are the same as those in Fig. 6. The desorption peaks of CO and H_2 were observed at 563 and 543 K, respectively. The desorption amounts of CO and H_2 is 25.3 and 15.2 μmol g^{-1}, respectively. CO_2 began to desorb at 553 K and had no peak below 773 K. Coexisted H_2O stabilized the surface formates. The backward decomposition (HCOO → OH + CO) was restrained by water, as shown by the shift of the CO desorption peak from 518 K (without water) to 563 K (with water). The decomposition selectivity (H_2/(H_2 + CO)) increased from 29 to 37.5% by the addition of water.

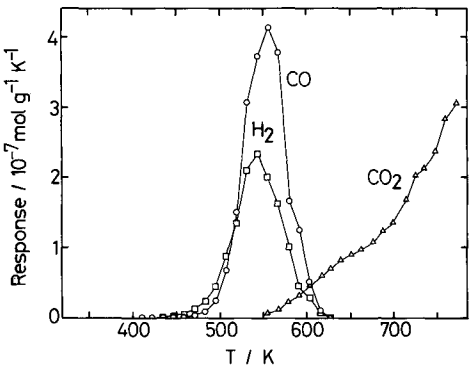

FIG. 7. TPD spectra of surface formates on CeO_2 (R, OH) under 0.67 kPa of water, (○) CO, (□) H_2, and (△) CO_2.

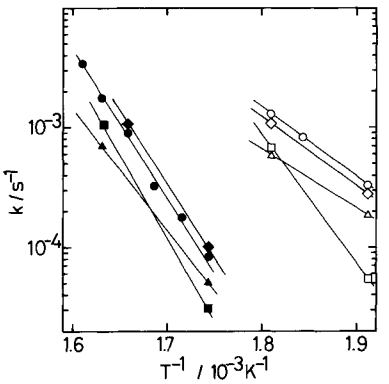

FIG. 8. Arrhenius plots for the decomposition of surface formate on CeO_2 (R, OD) and CeO_2 (RR, OD): (○) (□), and (△) represent $k_+ + k_-$, k_+, and k_- of the formate on CeO_2 (R, OD) in vacuum, respectively; (●), (■), and (▲) represent $k_+ + k_-$, k_+, and k_- of the formate on CeO_2 (R, OD) in vacuum, respectively; (●), (■), and (▲) represent $k_+ + k_-$, k_+, and k_- of the formate on CeO_2 (R, OD) in the presence of 0.66 kPa of water, respectively; (◇) and (◆) represent $k_+ + k_-$ of the formate on CeO_2 (RR, OD) in vacuum and in the presence of 0.66 kPa of water, respectively.

3. *Kinetics*

Arrhenius plots for the decomposition reaction of surface formates on CeO_2 (R, OD) and CeO_2 (RR, OD) in vacuum and in the presence of water vapor are shown in Fig. 8. Total rate constants for the decomposition ($k_+ + k_-$) were determined by IR, while the forward rate constant (k_+; HCOO → H_2 + CO_2) and backward rate constant (k_-; HCOO → OH + CO) were measured by mass spectrometry. k_+ and k_-, for the decomposition of formates on CeO_2 (R, OD) in presence of water, are ca. $\frac{1}{50}$ as large as those in vacuum. The activation energies for the forward (k_+) and backward (k_-) decomposition of surface formates were calculated to be 207 and 94 kJ mol^{-1}, respectively, in vacuum, and 264 and 193 kJ mol^{-1} in the coexistence of water vapor. The activation energy for the backward decomposition to produce OH + CO increased more than that for the forward decomposition to produce H_2 + CO_2. The sum of k_+ and k_- (individually determined by mass spectroscopy) agreed with the value of $k_+ + k_-$ (measured

TABLE 3

Rate Constants for the Decomposition of Surface Formates in the Presence of Various Coadsorbed Molecules[a]

Coadsorbed species	$k_+ + k_-$ (s^{-1})
None	3.15×10^{-3}
H_2O	1.75×10^{-4}
CH_3OH	6.09×10^{-4}
NH_3	8.81×10^{-4}
Pyridine	1.60×10^{-3}

[a] Decomposition rate constants were measured at 573 K.

by IR). The activation energies for surface formates on CeO_2 (RR, OD) in vacuum and in the presence of water were almost the same as the corresponding values on CeO_2 (R, OD): 137 kJ mol^{-1} in vacuum and 216 kJ mol^{-1} in presence of water. In vacuum, $k_+ + k_-$ for CeO_2 (RR, OD) is a little smaller than that for CeO_2 (R, OD), while in the presence of water vapor, $k_+ + k_-$ for CeO_2 (RR, OD) is a little larger than that for CeO_2 (R, OD).

Table 3 shows the rate constant ($k_+ + k_-$) for the decomposition of surface formates on CeO_2 (R, OD) in the coexistence of various molecules. The surface formates were stabilized and the rate constants of the decomposition decreased by the addition of H_2O, CH_3OH and NH_3 and pyridine.

Table 4 shows the forward rate constants

TABLE 4

Rate Constants for the Decomposition of Surface Formates under Various Isotope Combinations

Isotope combination	k_+ (s^{-1})
HCOO + H_2O	6.5×10^{-5}
HCOO + D_2O	4.8×10^{-5}
DCOO + H_2O	4.6×10^{-5}
DCOO + D_2O	3.1×10^{-5}

[a] Decomposition rate constants were measured at 573 K.

TABLE 5

Comparison of the Observed Reaction Rates for Catalytic WGSR and the Calcated Values from the Forward Decomposition Rates and the Amount of Surface Formates[a]

Reactant	T (K)	k_+[b]	M[c]	$k_+ + M$[d]	Reaction rate[d]
D_2O + CO	623	23	15	3.4	3.5
D_2O + CO	573	3.1	35	1.1	1.2
H_2O + CO	573	6.5	31	2.0	2.2

[a] $P(H_2O)$ or $P(D_2O)$ = 0.66 kPa and $P(CO)$ = 4.0 kPa.
[b] k_+ represents the rate constant for forward decomposition of formates in the presence of 0.66 kPa of water, in 10^{-5} s^{-1}.
[c] Amounts of surface formates with reaction conditions, in 10^{-6} mol g^{-1}.
[d] In 10^{-9} mol g^{-1} s^{-1}.

in the four different isotope combination. The isotope effects were observed with the hydrogen atom of both formate and water molecules.

The observed reaction rates for WGSR on CeO_2 reduced at 623 K were compared with the reaction rates calculated from the forward rate constants (k_+) and the adsorbed amounts of formates (M) in Table 5. The calculated reaction rates obtained by $k_+ \times M$ agreed with the observed reaction rate in various conditions. The catalytic reaction rate for WGSR over CeO_2 reduced at 723 K was about three times larger than that over CeO_2 reduced at 623 K. This difference in the reaction rate corresponds to the difference of the amount of surface formates.

DISCUSSION

1. Assignment of IR Bands

As shown in Figs. 1, 2, and 3, the set of the IR bands of {2156, 1540, and 1338 cm^{-1}}, {2135, 1560, and 1332 cm^{-1}}, and {1460, 1370, and 1044 cm^{-1}} behaved in a similar way, showing three different surface species. Besides these bands, IR bands at 1570 and 1510 cm^{-1} were observed. The behavior of the two bands was different from each other and independent of the behavior of

other bands. Thus, these bands are ascribed to two different species.

As shown in Table 2, the bands at 2156, 1540, and 1338 cm^{-1} and at 2140, 1560, and 1332 cm^{-1} shifted toward the higher frequency peaks at 2845, 1547, and 1358 cm^{-1} and at 2933, 1569, and 1358 cm^{-1}, respectively, by changing OD groups to OH groups. Thus, these bands are assigned to the bands for hydrogen-containing species, formate, produced from CO and OH (OD). Therefore, the IR bands of 2135–2156, 1540–1560, and 1332–1338 cm^{-1} are attributed to ν(CD), ν_{as}(OCO), and ν_s(OCO) of surface formates, respectively. The structures of the formates can be determined by the value of $\Delta\nu = \nu_{as}(OCO) - \nu_s(OCO)$ (*22*). When $\Delta\nu$ is larger than that of the free ion (ca. 220 cm^{-1}), the formate is unidentate formate. When $\Delta\nu$ is similar to that of the free ion, the formate is bridge type, and when $\Delta\nu$ is smaller than that of the free ion, the formate is bidentate type. Two kinds of formats existed on the CeO_2 surface, whose ν_{as}(OCO) and ν_s(OCO) are 1540 and 1338, and 1560 and 1332 cm^{-1}. The values of $\Delta\nu$ are 202 and 228 cm^{-1}, respectively. Thus, the formate with the bands of {ν(CD), ν_{as}(OCO), and ν_s(OCO)} = {2156, 1540, and 1338 cm^{-1}} is assigned to bidentate formate and the species with the bands of {2135, 1560, and 1332 cm^{-1}} is bridge formate. Li *et al.* studied adsorbed formic acid on CeO_2 and assigned bands at 2845, 1553, and 1362 cm^{-1} to ν(CH), ν_{as}(OCO), and ν_s(OCO) of bidentate formate, respectively (*24*). The wavenumbers of the peaks are similar to our result. They also investigated surface formate on CeO_2 formed by OH + CO and they observed bands at 2852, 1558, and 1329 cm^{-1}, which were assigned to be ν(CH), ν_{as}(OCO), and ν_s(OCO) of formate (*23*). This formate can be bridge-type formate because the value of $\Delta\nu$(229 cm^{-1}) is as large as that of the free formate. This difference may be caused by the difference of experimental condition. They evacuated the CeO_2 at 1100 K, which may cause a surface recombination to adapt to the forming of bridge formate.

IR bands at {1460, 1370, and 1044 cm^{-1}}, 1570 cm^{-1}, and 1510 cm^{-1} did not shift by the hydrogen isotope of OH group, suggesting that these bands are due to the species which do not contain hydrogen atoms. From this fact and their peak positions, the species can be assigned to surface carbonates or carboxylates. IR spectra of surface carbonates on oxide surfaces have extensively been studied (*14, 25–27*). In general, IR bands of 1420–1470 and 1350–1400 cm^{-1} are assigned to ν_{as}(OCO) and ν_s(OCO) of unidentate carbonate, and IR bands of 1550–1650, 1250–1300, and 1020–1050 cm^{-1} are assigned to ν(C═O), ν_{as}(OCO), and ν_s(OCO) of bidentate carbonate. IR bands of 1500–1550 and 1250–1350 cm^{-1} are assigned to ν_{as}(OCO) and ν_s(OCO) of carboxylate. Li *et al.* investigated on adsorbed carbonate and carboxylate on CeO_2 by IR and assigned the bands {1454, 1348, 1062, and 864 cm^{-1}}, {1562, 1286, 1028, and 854 cm^{-1}}, and {1510, and 1310 cm^{-1}} to unidentate carbonate, bidentate carbonate, and carboxylate, respectively (*27*). Their assignments agree with the general assignment of carbonate and carboxylate on oxide surfaces. Hence we assigned the IR bands at 1460, 1370, and 1044 cm^{-1} to ν_{as}(OCO), ν_s(OCO), and ν(CO) of unidentate carbonate, the bands at 1570 cm^{-1} to ν(C═O) of bidentate carbonate, and the bands at 1510 cm^{-1} to ν_{as}(OCO) of carboxylate.

In the region of ν(OD), two sharp bands at 2707 and 2681 cm^{-1} and two broad bands at 2590 and 2540 cm^{-1} were observed (Fig. 4a). In general, as the coordination number of the O atoms of hydroxyl groups increases, the frequency of ν(OH) decreases, and as for terminal hydroxyl groups, as the coordination number of bottom-metal ion increases, the frequency of ν(OH) increases (*19–21*). Thus the IR band at 2707 cm^{-1} is attributed to terminal OD groups, and IR bands at 2590 and 2540 cm^{-1} are attributed to hollow-site OD groups. As for the assignment of the band at 2681 cm^{-1} there are two possibilities, bridge OD groups and terminal OD groups whose bottom-Ce ion is coordi-

nated by less oxygen ions than the Ce ion for OD groups of 2707 cm^{-1}. The latter possibility can be excluded because the difference of frequency caused by the difference of the coordination number of bottom-metal ion for terminal OD groups is ca. 15 cm^{-1} and because the frequency difference between terminal and bridge OD groups is ca. 25 cm^{-1}, which is almost the same as the frequency difference (26 cm^{-1}) between 2707 and 2681 cm^{-1}. Hence, the band at 2681 cm^{-1} must be attributed to bridge OD groups. As shown in Figs. 4c–e, another IR band at 2692 cm^{-1} appeared when the sample was exposed to CO, followed by evacuation at higher temperatures. This new band is attributable to terminal OD groups whose O atoms weakly interact with adjacent Ce ions because the frequency was lower by 15 cm^{-1} than that of terminal OD groups, but the FWHM of this band was as large as 25 cm^{-1} by deconvolution (*21*). The 2692-cm^{-1} peak was also observed after surface formates were decomposed completely. The surface of CeO_2 is reduced by CO to form the oxygen vacancies, which may allow the O atom of the terminal hydroxyl to interact with the adjacent Ce ion.

2. Properties of Surface Species

When the reduced CeO_2 was exposed to CO at 300 or at 373 K, terminal OD groups decreased and new bands of ν(CD), ν_{as}(OCO), and ν_s(OCO) of formate appeared. This suggests that terminal OD groups react with CO to produce surface formates. This feature is similar to that observed with MgO(13) and ZnO(14). On unreduced CeO_2, surface formates were produced at 513 K. This difference can be explained as follows: for the formation of surface formates, coordinately unsaturated Ce ions are necessary. Surface formate cannot be produced on oxidized CeO_2 covered by oxygen atoms. On the reduced CeO_2, a part of surface O ions are removed by hydrogen as shown in Fig. 5. Surface oxygen on CeO_2 was removed as carbonates or carboxylates by the reaction with CO at elevated temperatures, with the subsequent formation of surface formates at the obtained unsaturated sites.

As discussed above, bridge and bidentate formates exist on CeO_2 (R, OD). When the sample was exposed to CO at 303 K, bridge formate was a major species. Bridge formates were converted to bidentate formates above 443 K. These results indicate that the transformation of bridge formate to bidentate formate requires an activation barrier, and the bidentate formate is present on the catalyst surface under WGSR.

The bands of bridge formates were broad (FWHM of ν_{as}(OCO): 40 cm^{-1}), while the bands of bidentate formate were sharp (FWHM of ν_{as}(OCO): 15 cm^{-1}), as shown in Fig. 2. The bidentate formates may be homogeneous by distributed on the surface. We think that broad bands of bridge formate are caused by weak interaction between the O atoms of bridge formate and Ce ions. CeO_2 crystal has a fluorite structure with a_0 = 0.541 nm and the Ce–Ce distance at CeO_2 (001) surface is 0.383 nm (*28*). On the other hand, the O–O distance of free-formate ion is 0.22 nm (*29*). The latter distance is shorter by 0.16 nm than the former. Thus, the surface bridge formates apt to convert into more stable bidentate formates.

H_2, CO, and CO_2 were desorbed in the TPD spectrum of surface formates (Fig. 6) when the intensity of ν(OD) peak increased. Thus, the surface formates decompose in two ways: one is a backward decomposition to OH + CO and the other is a forward decomposition to H_2 and CO_{2ad}. Desorption temperatures of H_2 and CO were different from each other and the activation energies for k_+ and k_- were also different as shown in Fig. 8. This is contrasted to the case of ZnO, on which the activation energies of k_+ and k_- were the same (*18*). The decomposition reaction on ZnO might have similar potential energy surfaces for the two ways. When the formates decomposed in vacuum, the intensity of the 1460- and 1370-cm^{-1} peaks increased in Fig. 2. Hence, CO_2 that was produced by the decomposition of the formates remained as unidentate carbonate on CeO_2.

The IR studies revealed that unidentate carbonate is a major species and small amounts of bidentate carbonate and carboxylate exist. Unidentate carbonates are stable and most of them remained on CeO_2 surface even at 750 K. On ZnO surface, unidentate carbonates and carboxylates are in equilibrium and carboxylates are more stable by 3 kJ mol^{-1} than unidentate carbonates in vacuum; carboxylates were converted to unidentate carbonates when water molecules are introduced to the ZnO surface (*14*). On the CeO_2 surface, however, such conversions were not observed. Desorption of unidentate carbonates was promoted by water. The desorption began at 710 K in vacuum, by whereas the desorption began at 550 K in the presence of water. The desorbed amount of CO_2 in the presence of water was 14 times larger than that in absence of water. This promoting effect may be caused by water dissociation at the site with the adsorbed unidentate carbonate similarly to the case of ZnO surface (*14*).

3. *Interaction of Surface Formate and Coadsorbed Water*

When a water molecule was admitted to the bidentate formate-covered CeO_2 surface, the rate of the decomposition of the surface formates decreased and the activation energy for the decomposition became large. As shown in Table 3 when various electron donors were introduced to the system, the decomposition rate of the formates ($k_+ + k_-$) decreases. Pyridine had the least effect, while H_2O most stabilized the formates. CH_3OH showed the medium effect among the four additives, and NH_3 shows less effect than CH_3OH. Thus, electron donor–acceptor pairs rather than electron donors alone may be sufficient to stabilize the surface formates. H_2O molecule can donate the lone-pair electrons of O atom to Ce cations and reversely, the positively charged H atom ($H^{\delta+}$) of H_2O withdraws electrons of the O ion of CeO_2 surface to decrease the ion diameter of the O ion, resulting in the stable interaction of the bidentate formate with Ce ion. The H_2O-stabilizing effect was similarly observed with CeO_2 reduced at 723 K as shown in Fig. 8, even though the amount of removed oxygen for CeO_2 reduced at 723 K was 20 times as large as that for CeO_2 reduced at 623 K. The surface oxygen removed by reduction at 723 K may be compensated by migration of oxygen from the bulk.

This kind of stabilization of surface formate by coadsorbed water has been observed on MgO surface (*13*) but not observed on ZnO surface (*14*). MgO (001) surface is also covered by O ions and coordinative unsaturarity of Mg ions on (001) surface is small. On the contrary, Zn ions on ZnO (1010) have two vacancy for coordination.

4. *Reaction Mechanism of WGSR on CeO_2*

As shown in Table 5, the rates of catalytic water–gas shift reaction (WGSR) agree with $k_+ \times M$ in various conditions, where k_+ and M represent the rate constant of the forward decomposition of bidentate formates and the amount of bidentate formates, respectively. These results demonstrate that bidentate formate is an intermediate of WGSR on CeO_2. On the other hands, the reaction rate of catalytic WGSR did not agree with the decomposition rate of unidentate carbonates. The decomposition rate of the unidentate carbonate determined by IR spectra was smaller than the catalytic WGSR rate, even though it was promoted by water. This contradiction is not clear, but unidentate carbonates may not uniformly be adsorbed on CeO_2 surface. Most of the carbonates are stable and only a small part of them are decomposed to CO_2 under the reaction conditions. This is supported by the TPD pattern (no peak) of the desorption of CO_2 in Fig. 7. In this case the rate of the decomposition determined by IR would not be correct because the IR peaks for those heterogeneous unidentate carbonates were not discriminated each other.

Isotope effects were observed on the hy-

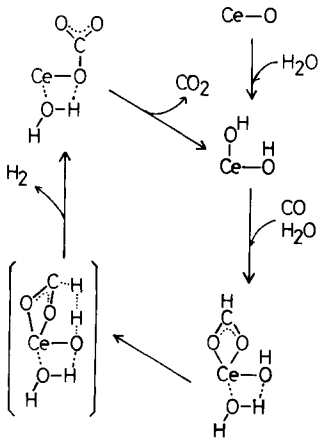

SCHEME 1. A reaction mechanism of catalytic water–gas shift reaction on CeO_2.

drogen atoms of both bidentate formate and hydroxyl groups. Hence the cleavage of both of CH and OH bonds is suggested to be involved in the rate-determining step. This is different from the cases of ZnO and MgO, where an isotope effect was observed on only the hydrogen of surface formate.

Scheme 1 shows the reaction mechanism for catalytic WGSR on CeO_2. Terminal OH groups on partially reduced CeO_2 react with CO to produce at first bridge formates as discussed above. The bridge formates were converted to bidentate formates at reaction temperatures, and this conversion was promoted by coadsorbed water. Bidentate formates are stabilized by coadsorbed water, and the decomposition of the formates is suppressed. The backward decomposition of the formates was more suppressed than the forward decomposition of the formates, changing the selectivity of the formate decomposition toward H_2 + CO_2 or OH + CO. To forward the decomposition of bidentate formate, the adjacent OH group (originally produced from the first water molecule) should contribute to produce H_2. By analogy to the reaction mechanism on ZnO, the bidentate formate is tilted and the C–H bond is bent, by which the hydrogen of the CH can interact with the hydrogen of the bridge OH groups at the transition state of reaction. In the transition state both C–H and O–H bands are elongated according to the hydrogen isotope effect. By the forward decomposition of the formate, unidentate carbonate is produced. The unidentate carbonate is stable at reaction temperature in vacuum. Water molecules promote the decomposition of the unidentate carbonate. The dissociation of water to produce two OH groups may be a driving force of this promotion.

Unlike to the surface formate on ZnO where the WGSR rate was enhanced by coadsorbed water (*14*), the bidentate formate on CeO_2 was not activated by coadsorbed water. Hence, the reactant-promoted effect is not observed on CeO_2. The stabilization of surface formates by coadsorbed water was also observed on MgO, whose (001) surface is covered by oxygen ions similarly to CeO_2 surface. However, reactive OH groups exist on edge sites (*21*), and the obtained formates were of bridge type under reaction conditions (*13*). On MgO, reactant-promoted WGSR proceeded (*13*). The catalytic WGSR proceeds on partially reduced CeO_2, where the coordinatively unsaturated Ce ions are produced after the removal of surface oxygen atoms. However, the arrangement of the vacant sites would be entirely different from those on edge sites of MgO and on the open sites of ZnO. Therefore, the nature and geometry of interaction between formate intermediate and coadsorbed water are expected to be different among CeO_2, MgO, and ZnO. ZnO, MgO, and CeO_2 are classified as basic oxides and their bulk nature may be not so different each other. Rather, the essential factors for the reactant-promoted catalysis seem to be ascribed to the surface structure (arrangement, defect, or edge) and/or surface oxygen density.

CONCLUSIONS

(1) Catalytic water–gas shift reaction (WGSR) on CeO_2 proceeded on the partially

reduced surfaces in the temperature range 510–620 K.

(2) There are four different OH groups on the CeO_2: terminal, bridge, and two hollow-site OH groups. The terminal OH groups reacted with CO to form bridge formates at 303–373 K.

(3) The bridge formates were converted to bidentate formates at reaction temperatures, and the conversion was promoted by the coexistence of water.

(4) The bidentate formates were stabilized by coadsorbed water, where the backward decomposition to OH + CO was suppressed. As a result, the forward decomposition of bidentate formate to H_2 + CO_2 was preferable in the coexistence of water.

(5) The rate of catalytic WGSR agrees with the rate of the decomposition of bidentate formate in various conditions, suggesting that the formate decomposition is rate-determining.

(6) In the transition state of the rate-determining step, the bond scission of both C–H (formate) and O–H (hydroxyl) is suggested to be involved.

(7) The bidentate formates were converted to unidentate carbonates. Its decomposition to CO_2 was promoted by coadsorbed water.

(8) The reactant-promoted catalysis was not observed with CeO_2 surface, unlike the cases of MgO and ZnO. The reason is ascribed to the nature and geometry of the interaction between formate intermediate and coadsorbed water molecule, associated with the surface structure/arrangement and/or surface oxygen density.

REFERENCES

1. Mendelovici, L., and Steinberg, M., *J. Catal.* **93,** 353 (1985).
2. Summers, J. C., and Ausen, S. A., *J. Catal.* **58,** 131 (1979).
3. Kiennemann, A., Breault, R., and Hindermann, J-P., *J. Chem. Soc. Faraday Trans. 1* **83,** 2119 (1987).
4. Mendelovici, L., and Stenberg, M., *J. Catal.* **96,** 285 (1985).
5. Mendelovici, L., and Stenberg, M., *Appl. Catal.* **4,** 237 (1982).
6. Oh, S. H., *J. Catal.* **124,** 477 (1990).
7. Nix, R. M., Judd, R. W., Lambert, R. M., Jennings, J. R., and Owen, G., *J. Catal.* **118,** 175 (1989).
8. Yao, H. C., Yu Yao, Y. F., *J. Catal.* **86,** 254 (1984).
9. Jin, T., Zhou, Y., Mains, G. J., and White, J. M., *J. Phys. Chem.* **91,** 1931 (1987).
10. Jin, T., Okuhara, T., Mains, G. J., and White, J. M., *J. Phys. Chem.* **91,** 3310 (1987).
11. Su, E. C., Montreuil, C. N., and Rothschild, W. G., *Appl. Catal.* **17,** 75 (1985).
12. Su, E. C., and Rothschild, W. G., *J. Catal.* **99,** 506 (1986).
13. Shido, T., Asakura, K., and Iwasawa, Y., *J. Catal.* **122,** 55 (1990).
14. Shido, T., and Iwasawa, Y., *J. Catal.* **129,** 343 (1991).
15. Scholten, J. J. F., Mars, P., Menon, P. G., and Hardereld, R. Van, *in* "Proceedings, 3rd International Congress on Catalysis, Amsterdam, 1964," Vol. 2, p. 881. Wiley, New York, 1965.
16. Ueno, A., Onishi, T., and Tamaru, K., *Trans. Faraday Soc.* **66,** 756 (1970).
17. Yamasita, K., Naito, S., and Tamaru, K., *J. Catal.* **94,** 357 (1985).
18. Noto, Y., Fukuda, K., Onishi, T., and Tamaru, K., *Trans. Faraday Soc.* **63,** 3081 (1967).
19. Tsyganenco, A. A., and Filimonov, V. N., *J. Mol. Struct.* **19,** 579 (1973).
20. Boehem, P. H., and Knözinger, H., *in* "Catalysis" (J. R. Anderson and M. Boudart, Eds.), Vol. 4, p. 39. Springer, Berlin, 1983.
21. Shido, T., Asakura, K., and Iwasawa, Y., *J. Chem. Soc. Faraday Trans. 1* **85,** 441 (1989).
22. Nakamoto, K., "Infrared and Raman Spectra of Inorganic and Coordination Compounds," 3rd ed. Wiley–Interscience, New York, 1987.
23. Li, C., Sakata, Y., Arai, T., Domen, K., Maruya, K., and Onishi, T., *J. Chem. Soc. Faraday Trans. 1* **85,** 1451 (1989).
24. Li, C., Domen, K., Maruya, K., and Onishi, T., *J. Catal.* **125,** 445 (1990).
25. Little, L. H., "Infrared Spectra of Adsorbed Species." Academic Press, New York, 1966.
26. Jin, T., Zhou, Y., Mains, G. J., and White, J. M., *J. Phys. Chem.* **91,** 5931 (1987).
27. Li, C., Sakata, Y., Arai, T., Domen, K., Maruya, K., and Onishi, T., *J. Chem. Soc Faraday Trans. 1* **85,** 929 (1989).
28. Wyckoff, R. W. G., "Crystal Structure," Vol. 1. InterScience, New York, 1951.
29. Marchese, F. T., Mehrotra, P. K., and Beveridge D. L., *J. Phys. Chem.* **86,** 2592 (1982).